

Simple Analytical Expression for the Peak-Frequency Shifts of Plasmonic Resonances for Sensing

Jianji Yang,[†] Harald Giessen,[‡] and Philippe Lalanne^{*,†}

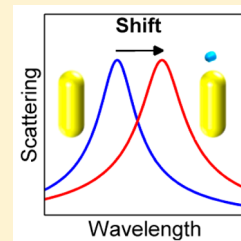
[†]Laboratoire Photonique Numérique et Nanosciences, Institut d'Optique d'Aquitaine, Université Bordeaux, CNRS, 33405 Talence, France

[‡]4th Physics Institute and Research Center SCoPE, University of Stuttgart, Pfaffenwaldring 57, 70550 Stuttgart, Germany

Supporting Information

ABSTRACT: We derive a closed-form expression that accurately predicts the peak frequency shift and broadening induced by tiny perturbations of plasmonic nanoresonators without critically relying on repeated electrodynamic simulations of the spectral response of nanoresonator for various locations, sizes, or shapes of the perturbing objects. In comparison with other approaches of the same kind, the force of the present approach is that the derivation is supported by a mathematical formalism based on a rigorous normalization of the resonance modes of nanoresonators consisting of lossy and dispersive materials. Accordingly, accurate predictions are obtained for a large range of nanoparticle shapes and sizes used in various plasmonic nanosensors even beyond the quasistatic limit. The expression gives quantitative insight and, combined with an open-source code, provides accurate and fast predictions that are ideally suited for preliminary designs or for interpretation of experimental data. It is also valid for photonic resonators with large mode volumes.

KEYWORDS: Refractive index sensing, surface plasmon resonance, quasi normal mode, nanoparticle, plasmonics



In recent years, metallic nanoparticles have gained a lot of attention and also witnessed successful applications in various fields of nanosciences. As their near-fields support strong and highly confined resonances, metallic nanoparticles can effectively convert local changes of refractive index into frequency shifts of the resonance.^{1,2} This property has driven considerable development in sensing technologies based on localized surface plasmon resonance (LSPR) of metallic nanoparticles,^{2,3} benefiting from significant advances in the detection of single metallic nanoparticles.^{4,5} Thanks to their small mode volume, LSPRs are suitable for achieving detection of ultrasmall refractive-index changes.^{2,6–8} Even single-molecule sensitivity has been recently achieved.^{9,10}

In this work, we derive an analytical formula that predicts the change $\Delta\tilde{\omega}$ of the complex-valued eigenfrequency $\tilde{\omega}$ of the LSPR, induced by a local near-field perturbation of resonant metallic nanoparticles. The derivation is motivated by the fact that the frequency shift $\text{Re}(\Delta\tilde{\omega})$ and the resonance broadening $-2/m(\Delta\tilde{\omega})$ are two quantities of fundamental importance for sensing applications.^{2,3,7} Yet another motivation is that the theoretical prediction of $\Delta\tilde{\omega}$ usually relies on tedious and repeated fully vectorial electromagnetic calculations for various parameters, such as the location, size, shape, or refractive index of the perturbation and that a simple and intuitive approach that is accurate for arbitrary nanoparticle sizes and shapes may help early designs or interpretation of experimental results and is essentially absent in the literature. Finally another motivation is that the derivation of an analytical formula accurate for photonic or plasmonic nanoresonators of arbitrary size and shape, potentially composed of lossy and dispersive materials, is of fundamental interest and has not been already established.

All these issues are addressed thanks to the introduction of the true resonance modes of lossy and dispersive resonant nanostructures and to the use of a rigorous normalization.¹¹ In passing, we remark that the present formula is also valid for photonic resonators and importantly for the practical case of nanoparticles that are placed on a substrate.

One of the major difficulties to derive such an analytical formula is the establishment of a “mode volume” (or mode normalization) for nanoresonators with strong energy dissipation resulting from either radiation leakage or absorption. The classical mode volume, which is defined with the electromagnetic energy stored in the cavity,^{12,13} is accurate only for high-Q dielectric cavities. The theoretical difficulty associated with dielectric cavities with strong leakage has been noted dating back to the early studies of optical microcavities^{12–15} and has reemerged in the context of plasmonic nanoresonators,^{16,17} in which absorption and dispersion additionally play an important role. Recently, a solid theoretical framework for the computation and normalization of the modes of lossy resonators has been established^{11,18} by transforming the resonance modes, which are morally scattering states, into square-integrable modes by using complex coordinate transforms.

The report is organized as follows. The closed-form expression for the frequency shift and resonance broadening is first derived. Then we explain how the resonance mode can be computed and normalized properly, for instance, with the

Received: February 25, 2015

Revised: April 1, 2015

Published: April 6, 2015



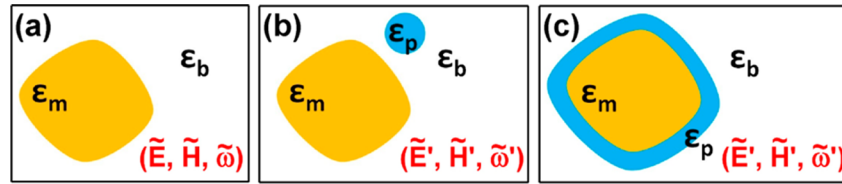


Figure 1. Schematic showing unperturbed and perturbed resonant metallic nanoparticles. (a) Bare metallic nanoparticle supporting a quasi-normal mode (QNM) $(\tilde{\mathbf{E}}, \tilde{\mathbf{H}})$ at eigenfrequency $\tilde{\omega}$. (b,c) Metallic nanoparticle perturbed by a small nanosphere or a thin shell, supporting a perturbed QNM $(\tilde{\mathbf{E}}', \tilde{\mathbf{H}}')$ at eigenfrequency $\tilde{\omega}'$. The permittivities of the metal, background medium, and perturbation are denoted by ϵ_m , ϵ_b , and ϵ_p , respectively.

open-source code in ref 19. We further outline the fundamental difference between the present work and previous theoretical works of the same kind.^{20–22} A thorough discussion is provided in the Supporting Information. Finally, we test the closed-form-expression accuracy for plasmonic nanoresonators of different sizes and shapes for perturbations with different shapes, refractive indices, and positions with respect to the nanoresonators and evidence that the formula is highly accurate for a broad panel of plasmonic sensors.

Master Equation. The closed-form expression for $\Delta\tilde{\omega}$ is simple. If we denote by $\tilde{\mathbf{E}}(\mathbf{r})$ the resonance mode (called as quasi-normal mode or QNM, hereafter) of the bare metallic nanoparticle and by $\tilde{\mathbf{E}}_{\text{app}}(\mathbf{r}) \approx \tilde{\mathbf{E}}(\mathbf{r})$ a slightly modified version of $\tilde{\mathbf{E}}(\mathbf{r})$ that takes into account local field corrections, the complex-frequency shift $\Delta\tilde{\omega}$ due to a local permittivity change $\Delta\epsilon(\mathbf{r}, \tilde{\omega})$, which may be a tensor for anisotropic media, reads as

$$\Delta\tilde{\omega} = -\tilde{\omega} \iiint_{V_p} \Delta\epsilon(\mathbf{r}, \tilde{\omega}) \tilde{\mathbf{E}}_{\text{app}}(\mathbf{r}) \cdot \tilde{\mathbf{E}}(\mathbf{r}) d^3\mathbf{r} \quad (1)$$

where the integral runs over the perturbation volume V_p . It will be shown that eq 1 provides accurate predictions for various shapes, sizes, and material properties of the metallic nanoresonator. The main force of eq 1 resides in the fact that once the QNM is calculated the shift is known analytically for any shape, size, position, or permittivity of the perturbation. Throughout the manuscript, the notation tilde is used to refer to QNMs.

At first glance, eq 1 resembles expressions obtained and successfully used in earlier works on resonance shifts for very high-Q dielectric resonators, such as microwave cavities,²³ microspheres,²⁴ or photonic crystal cavities,²⁵ and one may question the novelty of the work.

The main difference resides in the integrand used, a $\tilde{\mathbf{E}} \cdot \tilde{\mathbf{E}}$ product instead of a $\tilde{\mathbf{E}} \cdot \tilde{\mathbf{E}}^*$ product and, of course, in the mode normalization. Replacing $\tilde{\mathbf{E}} \cdot \tilde{\mathbf{E}}^*$ by $\tilde{\mathbf{E}} \cdot \tilde{\mathbf{E}}$ is not just a small modification but has profound implications:

- First, on a mathematical perspective, a resonance mode that leaks cannot be normalized with an $\tilde{\mathbf{E}} \cdot \tilde{\mathbf{E}}^*$ product since $\tilde{\mathbf{E}}(\mathbf{r})$ exponentially diverges as $|\mathbf{r}| \rightarrow \infty$.¹¹ Consistently, normalizations with $\tilde{\mathbf{E}} \cdot \tilde{\mathbf{E}}^*$ products are performed by considering arbitrarily finite integration domains in general with a real frequency.^{23–25}

- Second, for high-Q photonic resonators, the normalized resonance mode $\tilde{\mathbf{E}}(\mathbf{r})$ is nearly real, $\text{Im}(\tilde{\mathbf{E}})/\text{Re}(\tilde{\mathbf{E}}) = O(1/Q)$ ²⁶ and normalizations with either $\tilde{\mathbf{E}} \cdot \tilde{\mathbf{E}}$ or $\tilde{\mathbf{E}} \cdot \tilde{\mathbf{E}}^*$ on a finite integration domain are largely equivalent when estimating the frequency shift $\text{Re}(\Delta\tilde{\omega})$. However, $\tilde{\mathbf{E}} \cdot \tilde{\mathbf{E}}$ and $\tilde{\mathbf{E}} \cdot \tilde{\mathbf{E}}^*$ products provide distinctive predictions for $\text{Im}(\Delta\tilde{\omega})$. For instance, for a dielectric perturbation ($\Delta\epsilon$ real), the peak broadening $-2\text{Im}(\Delta\tilde{\omega})$ with $\tilde{\mathbf{E}} \cdot \tilde{\mathbf{E}}^*$ is always proportional to $\text{Im}(\Delta\tilde{\omega})$ with a proportionality factor that is real (as can be immediately seen by replacing $\tilde{\mathbf{E}}_{\text{app}}$ by $\tilde{\mathbf{E}}^*$ in eq 1), regardless of the mode profile

and the perturbation positions. This makes no sense, and consistently, peak-broadening predictions with analytical formulas are essentially absent in the literature on high-Q dielectric cavities to our knowledge. This difficulty is removed by the formula using $\tilde{\mathbf{E}} \cdot \tilde{\mathbf{E}}$ products. As will be shown in the following, peak broadenings are accurately predicted by eq 1 for low-Q plasmonic resonators. Further work should be undertaken to evaluate the accuracy of eq 1 for predicting the peak broadening of high-Q photonic resonators, but this evaluation remains out of the scope of the present contribution that focuses on plasmonic nanoresonators.

- Third, the phase of the resonant mode, which is ignored by $\tilde{\mathbf{E}} \cdot \tilde{\mathbf{E}}^*$ products matters in eq 1. For tiny perturbations, the phase variation over the spatial extent of the perturbation (i.e., phase-retardation effect) can be neglected, but for larger perturbations covering the entire surface of the resonator (see Figure 1c), phase-retardation effect cannot be neglected and should be incorporated in the integral over the perturbation volume. Phase-retardation effects are strikingly important for predicting light backscattering in optical waveguides in the presence of small fabrication imperfections for instance.²⁷

- Fourth, metallic resonators present particular challenges. Because the Q-factor is typically in the range between 10 and 100, $\text{Im}(\tilde{\mathbf{E}})$ cannot be neglected, and normalizations with either $\tilde{\mathbf{E}} \cdot \tilde{\mathbf{E}}$ or $\tilde{\mathbf{E}} \cdot \tilde{\mathbf{E}}^*$ provide distinct predictions for both $\text{Re}(\Delta\tilde{\omega})$ and $\text{Im}(\Delta\tilde{\omega})$. Additionally, because the field around the nanoparticle in free space diverges much faster than for dielectric cavities, the normalization issue becomes critical.^{14,17} Beyond the quasi-static limit, the field outside the nanoparticle matters critically for normalization and we will see that eq 1 provides accurate predictions for both $\text{Re}(\Delta\tilde{\omega})$ and $\text{Im}(\Delta\tilde{\omega})$.

- Finally, to further evidence the predictive force of the present formula, in the Supporting Information we make a thorough comparison of the present approach with a recent representative theoretical work of the same kind²² in which the relevant “mode” is calculated at the real-valued resonance frequency and the normalization involves $\tilde{\mathbf{E}} \cdot \tilde{\mathbf{E}}^*$ in the quasi-static approximation. Consistently with ref 22, we find that the quasi-static formula accurately predicts $\text{Re}(\Delta\tilde{\omega})$ for very small ($<\lambda/10$) resonators. However, we find that the quasi-static formula fails in predicting $\text{Im}(\Delta\tilde{\omega})$ for any resonator size and rapidly becomes inaccurate for predicting $\text{Re}(\Delta\tilde{\omega})$ as the resonator size is increased toward realistic values that are large enough to give sufficient scattering in plasmonic sensing technologies.^{6,9} In contrast, these severe limitations are not encountered with our eq 1, evidencing the importance of our universal and robust $\tilde{\mathbf{E}} \cdot \tilde{\mathbf{E}}$ treatment (including computation and normalization) of low-Q resonators.

Derivation of the Master Equation. To derive eq 1, let us start by considering two eigensolutions of source-free Maxwell’s equations. The first solution corresponds to the resonance mode of the bare metallic nanoparticle, $\nabla \times \tilde{\mathbf{E}} = -i\tilde{\omega}\mu(\tilde{\omega})\tilde{\mathbf{H}}$

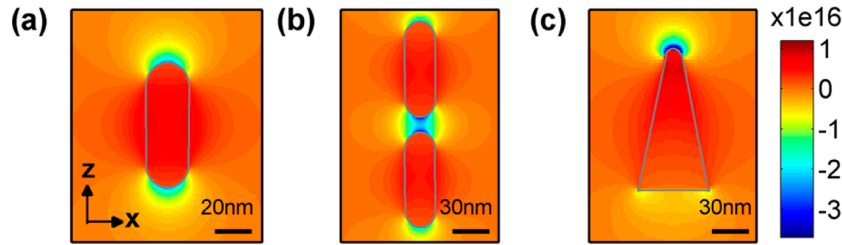


Figure 2. The electric field distribution $\text{Re}(\tilde{E}_z)$ of the normalized fundamental QNMs supported by three gold nanoresonators: (a) a single nanorod, (b) a nanorod dimer, and (c) a nanocone. The nanoresonators are placed in water ($\epsilon_b = 1.77$) and their dimensions is given in the main text. The associated eigenwavelengths, computed with the open-source COMSOL software in ref 19, are $\tilde{\lambda} = 2\pi c/\tilde{\omega} = 691.52-30.94i$, $756.44-47.12i$, and $805.31-40.28i$ nm, respectively. In the simulation, a Drude model $\epsilon_m = 1 - \omega_p^2/\omega^2 - i\omega\Gamma$ is adopted for the relative permittivity of gold with $\omega_p = 1.26 \times 10^{16} \text{ s}^{-1}$ and $\Gamma = 1.41 \times 10^{14} \text{ s}^{-1}$.

and $\nabla \times \tilde{\mathbf{H}} = i\tilde{\omega}\epsilon(\tilde{\omega})\tilde{\mathbf{E}}$, denoted as $(\tilde{\mathbf{E}}, \tilde{\mathbf{H}})$ with an eigenfrequency $\tilde{\omega}$, see Figure 1a. The second solution with an eigenfrequency $\tilde{\omega}'$, $\nabla \times \tilde{\mathbf{E}}' = -i\tilde{\omega}'\boldsymbol{\mu}(\tilde{\omega}')\tilde{\mathbf{H}}'$ and $\nabla \times \tilde{\mathbf{H}}' = i\tilde{\omega}'(\epsilon(\mathbf{r}, \tilde{\omega}') + \Delta\epsilon(\mathbf{r}, \tilde{\omega}'))\tilde{\mathbf{E}}'$, represents the resonance mode $(\tilde{\mathbf{E}}', \tilde{\mathbf{H}}')$ of the nanoresonator dressed by the perturbation (i.e., the permittivity change) $\Delta\epsilon(\mathbf{r}, \tilde{\omega}')$, see Figure 1b,c. Applying the Green–Ostrogradski formula to the vector $\tilde{\mathbf{E}}' \times \tilde{\mathbf{H}} - \tilde{\mathbf{E}}, \tilde{\mathbf{H}}'$, we obtain

$$\begin{aligned} & \iint_{\Sigma} (\tilde{\mathbf{E}}' \times \tilde{\mathbf{H}} - \tilde{\mathbf{E}} \times \tilde{\mathbf{H}}') \cdot d\mathbf{S} \\ &= -i \iiint_{\Omega} \{ \tilde{\mathbf{E}}' \cdot [\tilde{\omega}\epsilon(\tilde{\omega}) - \tilde{\omega}'(\epsilon(\tilde{\omega}') + \Delta\epsilon(\tilde{\omega}'))] \tilde{\mathbf{E}}' \\ & \quad - \tilde{\mathbf{H}} \cdot [\tilde{\omega}\boldsymbol{\mu}(\tilde{\omega}) - \tilde{\omega}'\boldsymbol{\mu}'(\tilde{\omega}')] \tilde{\mathbf{H}}' \} d^3\mathbf{r} \end{aligned} \quad (2)$$

where Σ is an arbitrary closed surface defining a volume Ω . In earlier work,¹¹ it was shown that the volume integral in eq 2 can be evaluated over the entire space, provided that the entire space is decomposed into two subdomains Ω_1 and Ω_2 with Ω_1 being a finite-volume real space that contains the metallic nanoparticle and Ω_2 being a surrounding space that can be implemented with perfectly matched layers (PMLs), which transform the exponentially diverging QNMs in real space into square-integrable modes with an exponential decay in Ω_2 ; see details in ref 11. Because of the exponential decay, the surface integral on the left-side of eq 2 becomes null and, assuming that $\Delta\tilde{\omega}$ is small so that we may use a first order expansion of the permittivity and permeability for $\omega \approx \tilde{\omega}$, eq 2 becomes

$$\begin{aligned} \frac{\Delta\tilde{\omega}}{\tilde{\omega}} &= \frac{\tilde{\omega}' - \tilde{\omega}}{\tilde{\omega}} = \\ &= \frac{\iiint_{V_p} \Delta\epsilon(\mathbf{r}, \tilde{\omega}) \tilde{\mathbf{E}}'(\mathbf{r}) \cdot \tilde{\mathbf{E}}(\mathbf{r}) d^3\mathbf{r}}{\iiint_{\Omega} \left\{ \tilde{\mathbf{E}}(\mathbf{r}) \cdot \frac{\partial[\omega\epsilon(\mathbf{r}, \omega)]}{\partial\omega} \tilde{\mathbf{E}}'(\mathbf{r}) - \tilde{\mathbf{H}}(\mathbf{r}) \cdot \frac{\partial[\omega\boldsymbol{\mu}(\mathbf{r}, \omega)]}{\partial\omega} \tilde{\mathbf{H}}'(\mathbf{r}) \right\} d^3\mathbf{r}} \end{aligned} \quad (3)$$

where $\Delta\epsilon(\mathbf{r}, \omega) = \epsilon_p(\mathbf{r}, \omega) - \epsilon_b(\mathbf{r}, \omega)$ with ϵ_p and ϵ_b the permittivities of perturbation and background medium. It is noteworthy that eq 3 is exact up to a first order in $\Delta\tilde{\omega}$.

To calculate the frequency shift $\Delta\tilde{\omega}$ using the sole knowledge of the unperturbed mode $\tilde{\mathbf{E}}$, we need to eliminate the unknown perturbed QNM $\tilde{\mathbf{E}}', \tilde{\mathbf{H}}'$. In the denominator, a very accurate assumption consists in considering that the perturbation modifies the QNM field distribution only locally in a volume approximately equal to V_p , and that the error induced by replacing $\tilde{\mathbf{E}}', \tilde{\mathbf{H}}'$ by $\tilde{\mathbf{E}}, \tilde{\mathbf{H}}$ into the denominator of eq 3 is negligible. Then using the QNM normalization

$$\iiint_{\Omega} \left\{ \tilde{\mathbf{E}} \cdot \frac{\partial[\omega\epsilon]}{\partial\omega} \tilde{\mathbf{E}} - \tilde{\mathbf{H}} \cdot \frac{\partial[\omega\boldsymbol{\mu}]}{\partial\omega} \tilde{\mathbf{H}} \right\} d^3\mathbf{r} = 1$$

(see ref 11), we obtain

$$\Delta\tilde{\omega} = -\tilde{\omega} \iiint_{V_p} \Delta\epsilon(\mathbf{r}, \tilde{\omega}) \tilde{\mathbf{E}}'(\mathbf{r}) \cdot \tilde{\mathbf{E}}(\mathbf{r}) d^3\mathbf{r} \quad (4)$$

To go further, we should estimate $\tilde{\mathbf{E}}'$ from $\tilde{\mathbf{E}}$. A crude approximation would consist in simply making $\tilde{\mathbf{E}}' \equiv \tilde{\mathbf{E}}$ in eq 4. However, we rather consider a better approximation, based on local-field corrections, $\tilde{\mathbf{E}}' \equiv \tilde{\mathbf{E}}_{\text{app}}$ as explained in the next section and finally obtain the master equation 1.

We remark that the QNM normalization relies on an analytical continuation in the complex space and can be implemented with PMLs in the domain Ω_2 . However, a much simpler and completely general method has been reported in ref 18. The method, which can be easily implemented with virtually all numerical Maxwell solvers, calculates normalized QNMs in a few (4–5) iterations that require a few minutes CPU-times. It is this method that we adopt hereafter for the numerical examples, using an open-source COMSOL code.¹⁹

In the Supporting Information, we provide a thorough evaluation of errors that occur when replacing $\tilde{\mathbf{E}}'$ by $\tilde{\mathbf{E}}_{\text{app}}$ or $\tilde{\mathbf{E}}$ in eq 3. We find that the error made in the denominator is completely negligible and that the dominant error that limits the accuracy of the master equation results from the replacement of $\tilde{\mathbf{E}}'$ in the numerator. In this regard, the error evaluation shows that much better accuracy is achieved with local-field corrections.

Local Field Corrections. In the following, we will consider the following two types of perturbations; a tiny nano-object placed in the near field of the metallic nanoresonator, see Figure 1b, and a thin shell surrounding a metallic nanoresonator, see Figure 1c. The former is important for nanoparticle detection, for instance,^{8,10,28–32} and the latter for biosensing applications^{32–34} or gas sensing.³⁵ For the former case, we adopt the polarizability tensor α of the nano-object to approximate $\tilde{\mathbf{E}}'$ from $\tilde{\mathbf{E}}$ and assume that the perturbed QNM-field $\tilde{\mathbf{E}}'(\mathbf{r})$ inside the nano-object (for $\mathbf{r} \in V_p$) is proportional to the unperturbed QNM-field $\tilde{\mathbf{E}}'(\mathbf{r})$ ³⁶

$$\tilde{\mathbf{E}}_{\text{app}}(\mathbf{r}) = \frac{\alpha\epsilon_b\tilde{\mathbf{E}}(\mathbf{r})}{[V_p\Delta\epsilon(\mathbf{r}, \tilde{\omega})]} \quad (5a)$$

The polarizability tensor can be calculated for any particle. For small spheres that will be tested numerically, it takes a simple form $\alpha = 4\pi R^3(\epsilon_p - \epsilon_b)/(\epsilon_p + 2\epsilon_b)$. For the shell case, we again assume that the perturbed QNM-field $\tilde{\mathbf{E}}'(\mathbf{r})$ inside the

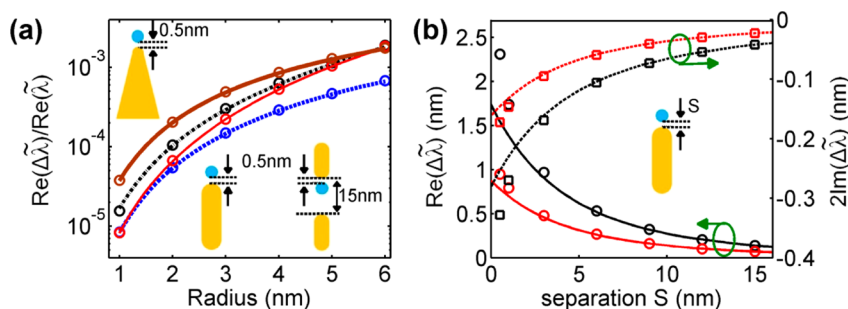


Figure 3. Resonance shifts of plasmonic nanostructures due to a perturbing nanosphere in aqueous environment ($\epsilon_b = 1.77$). (a) $\text{Re}(\Delta\tilde{\lambda})/\text{Re}(\tilde{\lambda})$ as a function of the nanosphere (protein, $\epsilon_p = 2.25$) radius for various nanoresonators. The sphere is placed 0.5 nm above the apex of the nanorod (blue dashed) or nanocone (brown thick). For the dimer, the nanosphere resides in the gap at 0.5 nm below the upper arm (black dotted-dash) or at the gap center (red thin). (b) $\text{Re}(\Delta\tilde{\lambda})$ and $2\cdot\text{Im}(\Delta\tilde{\lambda})$ as a function of the separation distance S between the nanorod and the perturbing nanosphere of radius $R = 3$ nm for nanospheres made of gold (black curves) and silicon (red curves, $\epsilon_p = 12.25$). In panels a and b, circle or square marks are obtained with fully vectorial calculation and curves are predicted with eq 1

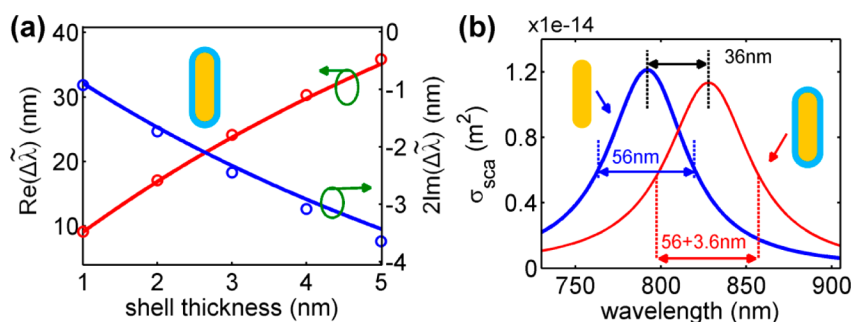


Figure 4. Resonance shift induced by the formation of a thin dielectric shell around a plasmonic nanorod in aqueous environment ($\epsilon_b = 1.77$). (a) $\text{Re}(\Delta\tilde{\lambda})$ (red) and $2\cdot\text{Im}(\Delta\tilde{\lambda})$ (blue) as a function of the shell thickness. Fully vectorial calculations and analytical predictions are represented by circles and solid curves. (b) Calculated scattering cross-section σ_{sca} as a function of the wavelength for a bare nanorod (blue) and the same nanorod covered by a 5 nm shell (red). In panels a and b, the shell permittivity is $\epsilon_p = 2.25$ and the rod radius and length are $R = 10$ nm and $L = 80$ nm.

shell (for $\mathbf{r} \in V_p$) is proportional to the unperturbed QNM-field $\tilde{\mathbf{E}}(\mathbf{r})$ with a proportionality factor settled by the field boundary conditions at the nanoresonator–shell interface

$$\tilde{\mathbf{E}}_{\text{app}}^{(T)}(\mathbf{r}) \approx \tilde{\mathbf{E}}^{(T)}(\mathbf{r}) \text{ and } \tilde{\mathbf{E}}_{\text{app}}^{(N)}(\mathbf{r}) \approx \frac{\epsilon_b}{\epsilon_p} \tilde{\mathbf{E}}^{(N)}(\mathbf{r}) \quad (5b)$$

where the superscripts (T) and (N) refer to tangential and normal field components. This modified first-order Born approximation is known to be very accurate for small shell thicknesses; see, for instance, a related theoretical study on slow light propagation in photonic-crystal waveguides²⁷ in the presence of small fabrication imperfections.

Quantitative Numerical Tests of the Master Equation.

For the numerical tests, we consider three types of metallic nanoresonators: a cylindrical gold nanorod (radius $R = 15$ nm and length $L = 90$ nm), a dimer composed by two identical cylindrical gold nanorods ($R = 15$ nm and $L = 90$ nm, gap size 15 nm) and a gold nanocone ($L = 100$ nm and $R = 27.5$ nm at bottom). The apexes of the nanorods and the nanocone are rounded (the nanorod apexes are hemispheres with the same radius as the cylinder and the nanocone apex is rounded with a radius of curvature $R = 7.5$ nm). The nanoresonators are assumed to be surrounded by water ($\epsilon_b = 1.77$). The z -component of the electric field of the fundamental QNMs are shown in Figure 2. Hot spots in water show up with a blue color.

To test the accuracy of eq 1, we compare the resonance shift $\Delta\tilde{\omega}$ predicted with eq 1 to the exact shift value $\Delta\tilde{\omega}_{\text{exact}}$ computed as the difference of the eigenwavelengths of the

perturbed and the unperturbed QNMs, both obtained with the open-source COMSOL code¹⁹ with two independent computations. The fully vectorial approach adopted here to obtain $\Delta\tilde{\omega}_{\text{exact}}$ is equivalent to the usual approach (more details can be found in the discussion about the last example), which consists in comparing the spectral responses (e.g., spectra of the absorption or extinction) of a perturbed resonator and an unperturbed resonator, but it is more efficient from numerical perspectives and is also more accurate for estimating small changes of the resonance width.

Figure 3a shows the wavelength shifts induced by the presence of a protein nanosphere ($\epsilon_p = 2.25$) located in the hot spots of the three metallic nanoresonators at a 0.5 nm separation distance from the metal surface. These situations are encountered in single-molecule sensing experiments, where the analyte can be chemically adsorbed to the nanoresonator surface with an analyte–metal spacing of ~ 1 nm.^{9,10} The best sensitivity is obtained for the nanocone (brown-thick curve). This is straightforwardly deduced from the hot-spot intensities in Figure 2, because the brighter spot is achieved at the nanocone apex. This underlines the importance of a proper disposal of QNM normalization. The dimer performance is tested for two nanosphere locations in the gap, either 0.5 nm below the upper arm (black curve) or exactly at the gap center (red curve). On the whole, the dimer performance is better than that of its constituting element, the single nanorod (blue curve); remarkably, it becomes as sensitive as the nanocone. This is again easily understood from Figure 2; close to the nanocone apex, the QNM near-field is the strongest one, but it

also the most confined so that a balance is achieved for relatively large nanospheres. In general, the agreement between the analytical predictions obtained with eq 1 and the fully vectorial calculations is excellent in Figure 3a. We have performed additional tests for nanorods with different dimensions (not shown) and similar agreement was achieved; we found that as the size of the nanorod apex increases, the sensitivity decreases.

Figure 3b reports additional tests performed for perturbing nanospheres of high permittivity $|\epsilon_p|$, such as those used for the sensing applications in which target analytes are labeled by high-permittivity nanoparticles.^{28,30} Two spherical nanoparticles with radius $R = 3$ nm are considered; one is made of gold ($\epsilon_p(\tilde{\omega}) = -20.45 + 0.81i$ at resonance) and the other one of silicon ($\epsilon_p = 12.25$). The shifts are calculated as a function of the separation distance to the nanorod apex, see inset. Again the agreement is excellent at least for separation distances S larger than 1 nm. For $S < 1$ nm, the local field correction of eq 5a is no longer valid. As shown by an inspection of the near-field distribution $E^7(\mathbf{r})$ of the perturbed nanorod, the failure of the local field correction can be ascribed to the emergence of strong gap resonance^{37,38} confined between the nanorod apex and the high-permittivity nanosphere for $S < 1$ nm. We remark that though the change of the resonance width in terms of $2 \cdot \text{Im}(\Delta\tilde{\lambda})$ is small, the analytical formula is accurate enough to capture this subtle information.

Figure 4 summarizes the tests made for protein ($\epsilon_p = 2.25$) shells adsorbed on a gold nanorod ($R = 10$ nm, $L = 80$ nm, and $\tilde{\lambda} = 792.55 - 28.02i$ nm) in aqueous environment ($\epsilon_b = 1.769$). This corresponds to sensing techniques for which a self-assembled-monolayer analyte envelopes a metallic nanoparticle.^{6,32,33} In Figure 4a, predictions obtained with eq 1 containing the local field correction of eq 5b are plotted as solid curves; again quantitative agreement with fully vectorial calculations (circles) is achieved even for shell thicknesses as large as a few nanometers. The calculation indicates a nearly linear dependence of $\text{Re}(\Delta\tilde{\lambda})$ and $\text{Im}(\Delta\tilde{\lambda})$ on the shell thickness, consistently with experimental observations.¹⁶ In Figure 4b, we show the scattering cross-section spectra of the bare nanorod (blue) and the perturbed nanorod (5 nm shell, red). The spectra are calculated using COMSOL multiphysics. By fitting with a Lorentzian function, we find a red shift of 36 nm and a resonance broadening of ~ 3.6 nm. These values, which are inferred from spectrum characteristics that are typically encountered in real experiments, are fully consistent with the predictions of the closed-form expression $\text{Re}(\Delta\tilde{\lambda}) \approx 35.1$ nm and $-2 \cdot \text{Im}(\Delta\tilde{\lambda}) \approx 3.4$ nm, offering a posteriori validation of the pure QNM approach (namely, the fully vectorial computations of frequency shift) used for testing the accuracy of the prediction of closed-form expression in Figures 3a,b and 4a.

Finally, throughout this paper we consider single mode cases, where the spectral responses of the metallic nanoresonators are driven solely by a single resonance mode and the scattering or absorption spectra are basically Lorentzian just as the ones in Figure 4b. In multimode cases, on the other hand intricate Fano-like spectral lineshapes^{11,39–42} can be observed because the perturbation may affect several QNMs, leading to complicated deformation in the spectral lineshapes. One may extend the current perturbation approach to these cases,¹¹ by considering the interaction of the perturbation with each QNM and obtain more physical insight. However, in this case one must be cautious with the concepts of frequency shift and peak

broadening. Additionally, we consider nanospheres, as isolated perturbing nanoparticles, with a well-known polarizability to test the analytical formula; however, in general one should ideally adopt proper polarizabilities for perturbing nanoparticles with different shapes to determine the local field correction.³⁶

Conclusion. We have derived a closed-form expression to predict the localized-plasmon-resonance shift and broadening of metallic nanoresonators induced by tiny perturbations of the resonator near-fields. The successful derivation benefits from a recent theoretical advance in the computation and normalization of the resonance modes of lossy nanoresonators. Verification of the accuracy of closed-form expression for various sensing configurations has been performed by comparison with fully vectorial calculations of the complex eigenfrequencies of the perturbed nanoresonators. We emphasize that the present approach is not stringently restricted by the size or shape of the nanoresonators or perturbations and it may be used for nanoresonators laying on a substrate. Finally, it is worth emphasizing that, provided that one is equipped with a Maxwell QNM solver such as the one we have used in this work, the resonance shift is known analytically. It would be interesting to consider extension of the present work to nanoresonators that operate by combining several resonances, such as complex systems sustaining Fano resonances.⁴³

■ ASSOCIATED CONTENT

Supporting Information

(1) Comparison of the present master equation with a quasi-static formula recently published.²² (2) Analysis of the errors resulting from the approximations made to derive the master equation. This material is available free of charge via the Internet at <http://pubs.acs.org>.

■ AUTHOR INFORMATION

Corresponding Author

*E-mail: philippe.lalanne@institutoptique.fr.

Notes

The authors declare no competing financial interest.

■ ACKNOWLEDGMENTS

J.Y. and P.L. thank M. Perrin, C. Sauvan, and J. P. Hugonin for fruitful discussions and help. Part of the study was carried out with financial support from “the Investments for the future” Programme IdEx Bordeaux–LAPHIA (ANR-10-IDEX-03-02). H.G. thanks the ERC (Complexplas), the BMBF, DFG, and BW Stiftung for support.

■ REFERENCES

- (1) Lal, S.; Link, S.; Halas, N. J. *Nat. Photonics* **2007**, *1*, 641–648.
- (2) Stewart, M. E.; Anderton, C. R.; Thompson, L. B.; Maria, J.; Gray, S. K.; Rogers, J. A.; Nuzzo, R. G. *Chem. Rev.* **2008**, *108*, 494–521.
- (3) Doria, G.; Conde, J.; Veigas, B.; Giestas, L.; Almeida, C.; Assunção, M.; Rosa, J.; Baptista, P. V. *Sensors* **2012**, *12*, 1657–1687.
- (4) van Dijk, M. A.; Lippitz, M.; Orrit, M. *Acc. Chem. Res.* **2005**, *38*, 594–601.
- (5) Zijlstra, P.; Orrit, M. *Rep. Prog. Phys.* **2011**, *74*, 106401.
- (6) Anker, J.; Paige Hall, W.; Lyandres, O.; Shah, N.; Zhao, J.; Van Duyne, R. P. *Nat. Mater.* **2008**, *7*, 442–453.
- (7) Mayer, K. M.; Hafner, J. H. *Chem. Rev.* **2011**, *111*, 3828–3857.
- (8) Liu, N.; Tang, M. L.; Hentschel, M.; Giessen, H.; Alivisatos, A. P. *Nat. Mater.* **2011**, *10*, 631–636.

- (9) Ament, I.; Prasad, J.; Henkel, A.; Schmachtel, S.; Sönnichsen, C. *Nano Lett.* **2012**, *12*, 1092–1095.
- (10) Zijlstra, P.; Paulo, P. M. R.; Orrit, M. *Nat. Nanotechnol.* **2012**, *7*, 379–382.
- (11) Sauvan, C.; Hugonin, J.-P.; Maksymov, I. S.; Lalanne, P. *Phys. Rev. Lett.* **2013**, *110*, 237401.
- (12) Gérard, J.-M. *Top. Appl. Phys.* **2003**, *90*, 269–314.
- (13) Chang, R. K.; Campillo, A. J. *Optical Processes in Microcavities*; World Scientific: Singapore, 1996.
- (14) Kristensen, P. T.; van Vlack, C.; Hughes, S. *Opt. Lett.* **2012**, *37*, 1649.
- (15) Muljarov, E. A.; Doost, M. B.; Langbein, W. 2014, arXiv:1409.6877 [cond-mat.mes-hall]. (accessed Oct 2014).
- (16) Maier, S. A. *Opt. Quantum Electron.* **2006**, *38*, 257.
- (17) Koenderink, A. F. *Opt. Lett.* **2010**, *35*, 4208.
- (18) Bai, Q.; Perrin, M.; Sauvan, C.; Hugonin, J.-P.; Lalanne, P. *Opt. Exp.* **2013**, *21*, 27371–27382.
- (19) See the section COMSOL MODELS: quasi-normal mode calculation on the webpage <https://www.lp2n.institutoptique.fr/Membres-Services/Responsables-d-equipe/LALANNE-Philippe> (accessed June 2014).
- (20) Unger, A.; Kreiter, M. *J. Phys. Chem. C* **2009**, *113*, 12243–12251.
- (21) Antosiewicz, T. J.; Apell, S. P.; Claudio, V.; Käll, M. *Opt. Exp.* **2012**, *20*, 524–533.
- (22) Zhang, W.; Martin, O. J. F. *ACS Photonics* **2015**, *2*, 144–150.
- (23) Waldron, R. A. *Proc. Inst. Electr. Eng.* **1960**, *107C*, 272.
- (24) Arnold, S.; Khoshsima, M.; Teraoka, I.; Holler, S.; Vollmer, F. *Opt. Lett.* **2003**, *28*, 272.
- (25) Koenderink, A. F.; Kafesaki, M.; Buchler, B. C.; Sandoghdar, V. *Phys. Rev. Lett.* **2005**, *95*, 153904.
- (26) Lalanne, P.; Sauvan, C.; Hugonin, J.-P. *Laser Photon. Rev.* **2008**, *2*, 514–526.
- (27) Wang, B.; Mazoyer, S.; Hugonin, J.-P.; Lalanne, P. *Phys. Rev. B* **2008**, *78*, 245108.
- (28) Sannomiya, T.; Hafner, C.; Voros, J. *Nano Lett.* **2008**, *8*, 3450–3455.
- (29) Zhang, W.; Huang, L.; Santschi, C.; Martin, O. J. F. *Nano Lett.* **2010**, *10*, 1006–1011.
- (30) Shopova, S. I.; Rajmangal, R.; Holler, S.; Arnold, S. *Appl. Phys. Lett.* **2011**, *98*, 243104.
- (31) Mayer, K. M.; Hao, F.; Lee, S.; Nordlander, P.; Hafner, J. H. *Nanotechnology* **2010**, *21*, 255503.
- (32) Malinsky, M.; Lance Kelly, K.; Schatz, G. C.; Van Duyne, R. P. *J. Am. Chem. Soc.* **2011**, *123*, 1471–1482.
- (33) McFarland, A.; Van Duyne, R. P. *Nano Lett.* **2003**, *3*, 1057–1062.
- (34) Ahijado-Guzmán, R.; Prasad, J.; Rosman, C.; Henkel, A.; Tome, L.; Schneider, D.; Rivas, G.; Sönnichsen, C. *Nano Lett.* **2014**, *14*, 5528–5532.
- (35) Tittl, A.; Giessen, H.; Liu, N. *Nanophotonics* **2014**, *3*, 157.
- (36) Harrington, R. F. *Time-Harmonic Electromagnetic Fields*; Wiley-IEEE Press: New York, 2001; Chapter 7.
- (37) Oulton, R. F.; Sorger, V. J.; Genov, D. A.; Pile, D. F. P.; Zhang, X. *Nat. Photonics* **2008**, *2*, 496–500.
- (38) Choo, H.; Kim, M. K.; Staffaroni, M.; Seok, T.; Bokor, J.; Cabrini, S.; Schuck, P. J.; Wu, M. C.; Yablonovitch, E. *Nat. Photonics* **2012**, *6*, 838–844.
- (39) Hao, F.; Sonnefraud, Y.; Van Dorpe, P.; Maier, S. A.; Halas, N. J.; Nordlander, P. *Nano Lett.* **2008**, *8*, 3983–3988.
- (40) Liu, N.; Langguth, L.; Weiss, T.; Kästel, J.; Fleischhauer, M.; Pfau, T.; Giessen, H. *Nat. Mater.* **2009**, *8*, 758–762.
- (41) Liu, N.; Weiss, T.; Mesch, M.; Langguth, L.; Eigenthaler, U.; Hirscher, M.; Sönnichsen, C.; Giessen, H. *Nano Lett.* **2010**, *10*, 1103–1107.
- (42) Gallinet, B.; Martin, O. J. F. *ACS Nano* **2013**, *7*, 6978–6987.
- (43) Luk'yanchuk, B.; Zheludev, N. I.; Maier, S. A.; Halas, N. J.; Nordlander, P.; Giessen, H.; Chong, C. T. *Nat. Mater.* **2010**, *9*, 707–715.